From *Physics of The Living State*
(Edited by T. Musha and Y. Sawada, Ohmsha, 1994)

3-6 Complex Dynamical Behaviors in Cilia and Flagella: Motility and Mechanosensitivity

Masatoshi Murase

Yukawa Institute for Theoretical Physics
Kyoto University
e-mail: murase@yukawa.kyoto-u.ac.jp

1. Introduction

Next to muscle (as discussed in Essays 3-4 and 3-5) the best understood type of living motile organelles is cilia and flagella.* They are hair-like projections and have an identical structure called the *"9+2" axoneme* [1]. These different names are merely a matter of definition, as illustrated in Figure 1. Cilia and flagella are found on many kinds of eukaryotic cells such as spermatozoa, protozoa (e.g., *Paramecium*), and ciliated epithelial cells of metazoa (e.g., tracheal ciliated epithelia) [2], [3]. Their primary function is to move single cells through a fluid for locomotion or to move fluid over the fixed cell surface for transport (e.g., mucous transport in the lung).

Motility of cilia and flagella results from the active sliding between *outer doublets* powered by *dynein-tubulin* mechanochemical cycles similar to *myosin-actin* cycles in muscle [4]–[6]. While muscle shows only one-dimensional contraction [7] and *oscillations* [8], cilia and flagella exhibit more complex dynamical behaviors such as symmetric base-to-tip bend propagation [9], reversal of its direction [10], [11], *intermittent* swimming with *stopping* and *starting* transients [12], asymmetric repetitive beats with *effective* and *recovery* strokes [13], rest or *quiescence* at particular stroke position [14], [15], and *excitability* with *directional mechanosensitivity* [16].

The problem which remains unresolved for over 100 years, is to understand how cilia and flagella produce such a variety of spatio-temporal bending patterns. Various attempts have been made not to account for the overall dynamical behaviors mentioned above, but rather to model some of the specific modes [17]–[30].

I shall attempt to solve the above problem based upon recent theoretical studies [31]–[36]. In Section 2 a functional unit of cilia and flagella is modelled. Many such functional units are arranged in one-dimensional space as a model of flagella in Section 3 and of cilia in Section 4. This model gives rise to a rich dynamical behavior, which is interpreted in terms of the properties of "nonlinear distributed systems" in Section 5.

---

* Confusingly, bacterial flagella share the same name as those of eukaryotes. They are, however, completely different in the structure and function.

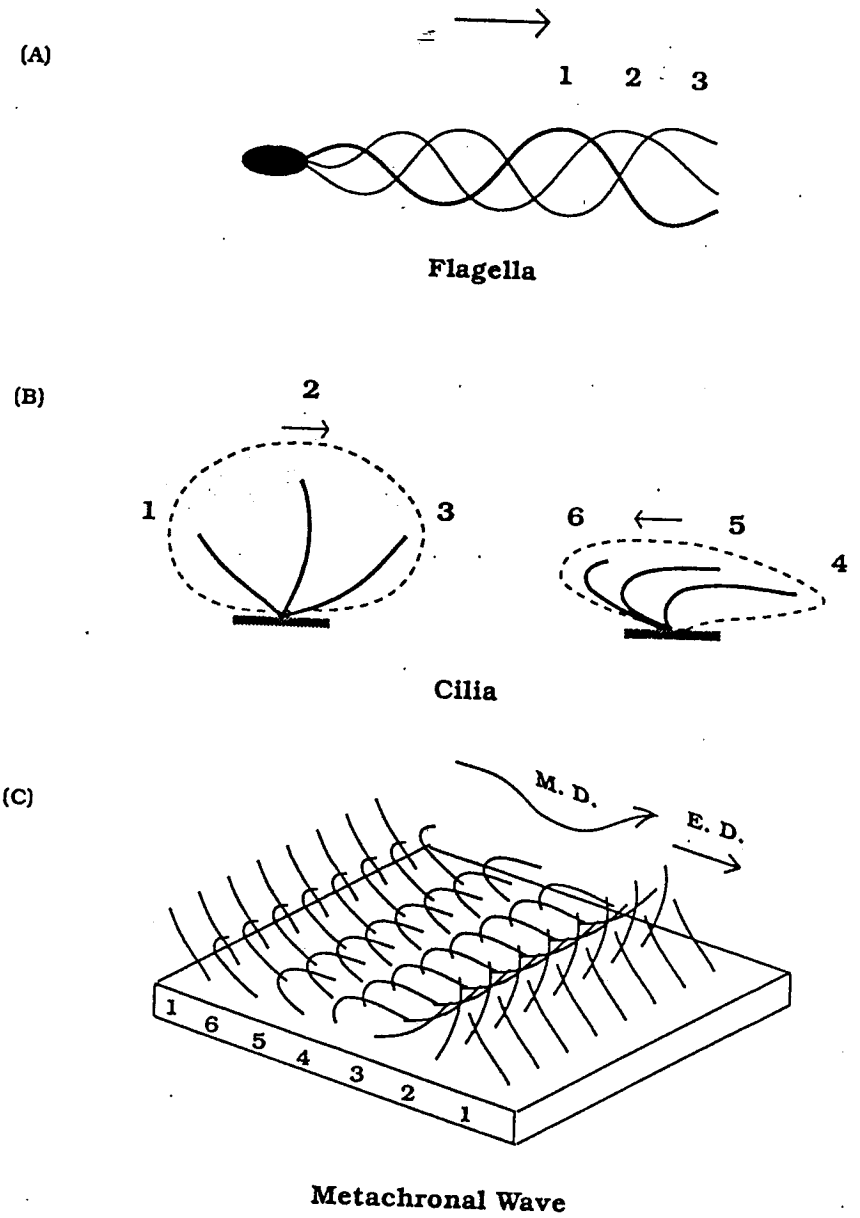

Figure 1. Typical beating patterns of flagella and cilia. (A): Flagella are very long and occur alone or in small numbers per cell. Sperm tails provide a typical example of flagella. They generally show symmetric base-to-tip bend propagation (1–3) to move water along the flagellar axis as indicated by the arrow. As a result, the sperm head is propelled forward. (B): Cilia are short and occur in large numbers per cell. They show asymmetric beat cycle with the effective (1–3) and recovery stroke (4–6). During the effective stroke, the extended cilium moves toward one side by making an "oar-like" movement. During the recovery stroke, the cilium moves back by propagating a bend from the base to tip. The arrows indicate the water flow caused by activity of cilia. The shaded area is a rough image of the extent of flow influenced by each stroke. (C): When cilia occur in large numbers, the movements of adjacent cilia are synchronized via hydrodynamic interactions to beat *in-phase* along one direction, but *out-of-phase* along another direction. Waves of ciliary movements, known as *metachronal waves*, propagate along this out-of-phase direction. Through the metachronal coordination of ciliary activity, ciliated systems seem to achieve higher efficiency for the propulsion of fluids than could be achieved by random movement of the cilia. The numbers assigned to the various stages of the beat cycle are the same for those in panel (B). E. D. and M. D. indicate the direction of the effective stroke and that of the propagation of the metachronal wave, respectively. After Murase [33].

2. Functional Unit of Cilia and Flagella

The active sliding between each pair of outer doublets only occurs in one direction [5] due to a *unidirectional* dynein power stroke [6]. Because of the closed ring of doublets, backward sliding of the same pair of doublets is passively induced by active sliding of other pairs in the axoneme. Assuming that bending occurs in a single plane, the 9 + 2 axoneme is simplified by two opposing dynein subsystems I and II (Fig. 2).

Each dynein subsystem assumes two important properties: *hysteresis* and *excitability*. Hysteresis arises when a dynein is either turned "on" or "off", depending on the "history" of the dynein behavior. This history-dependent characteristic refers to the unidirectional dynein power stroke. Let x denote the sliding as a dimensionless distance (changing from 0 to 1) between a dynein on one doublet and a reference point on its adjacent doublet, n_{I} (or n_{II}) the fraction of subsystem I (or II) in the "on" state with force F_{I} (or F_{II}). Then the hysteresis is described by the *binary* function of x (Fig. 3, A). S_1 and S_2 are the "on" and "off" *switching points* for subsystem I and the reverse is true for subsystem II (i.e., $n_{\mathrm{I}} + n_{\mathrm{II}} = 1$).

Excitability is represented by a cubic (or a modified cubic) force-distance function for the "on" state which crosses the x-axis three times with a negative slope (Fig. 3, B). There are threshold values x_c and x_c' in subsystem I and II, respectively. Suppose that subsystem I is in the "on" state. For $x < x_c$, a dynein persists in the "resting" state ($x \rightarrow x_1$), while for $x > x_c$, a dynein undergoes "power stroke" ($x \rightarrow x_2$). If subsystem II is in the "on" state, then the reverse is obtained with respect to sliding direction.

Now consider a functional unit consisting of two opposing subsystems and passive elastic links. The total shear force, F, is:

$$F = F_{\mathrm{I}}(x)n_{\mathrm{I}}(x) + F_{\mathrm{II}}(x)n_{\mathrm{II}}(x) - K_e(x - x_0), \tag{1}$$

where K_e is the force constant for the passive elastic elements (e.g., *nexin links* which may exert a restoring force proportional to their distortion), and x_0 is their location in the unstretched state.

If this functional unit is subject to internal viscous shear force, $\gamma\, \mathrm{d}x/\mathrm{d}t$ (γ is the internal viscous shear resistance*), the system obeys the force-balance equation

$$\gamma \frac{\mathrm{d}x}{\mathrm{d}t} = F. \tag{2}$$

When K_e is small enough (say 0), this system exhibits *bi-stability*. Either a stable state at $x = x_1$ or x_2 can be present, depending on the initial sliding. When x_0 is located in the unstable region and K_e is large enough, this system shows oscillations. Therefore, the functional unit has potentially excitability and oscillations.

* The internal viscous shear resistance is tentatively considered to allow force balance at a finite sliding velocity. In the flagellar and ciliary simulations, however, the internal viscosity is replaced by the external viscosity (see Eq. (3)).

2. Functional Unit of Cilia and Flagella

The active sliding between each pair of outer doublets only occurs in one direction [5] due to a *unidirectional* dynein power stroke [6]. Because of the closed ring of doublets, backward sliding of the same pair of doublets is passively induced by active sliding of other pairs in the axoneme. Assuming that bending occurs in a single plane, the 9 + 2 axoneme is simplified by two opposing dynein subsystems I and II (Fig. 2).

Each dynein subsystem assumes two important properties: *hysteresis* and *excitability*. Hysteresis arises when a dynein is either turned "on" or "off", depending on the "history" of the dynein behavior. This history-dependent characteristic refers to the unidirectional dynein power stroke. Let x denote the sliding as a dimensionless distance (changing from 0 to 1) between a dynein on one doublet and a reference point on its adjacent doublet, n_{I} (or n_{II}) the fraction of subsystem I (or II) in the "on" state with force F_{I} (or F_{II}). Then the hysteresis is described by the *binary* function of x (Fig. 3, A). S_1 and S_2 are the "on" and "off" *switching points* for subsystem I and the reverse is true for subsystem II (i.e., $n_{\mathrm{I}} + n_{\mathrm{II}} = 1$).

Excitability is represented by a cubic (or a modified cubic) force-distance function for the "on" state which crosses the x-axis three times with a negative slope (Fig. 3, B). There are threshold values x_c and x_c' in subsystem I and II, respectively. Suppose that subsystem I is in the "on" state. For $x < x_c$, a dynein persists in the "resting" state ($x \rightarrow x_1$), while for $x > x_c$, a dynein undergoes "power stroke" ($x \rightarrow x_2$). If subsystem II is in the "on" state, then the reverse is obtained with respect to sliding direction.

Now consider a functional unit consisting of two opposing subsystems and passive elastic links. The total shear force, F, is:

$$F = F_{\mathrm{I}}(x)n_{\mathrm{I}}(x) + F_{\mathrm{II}}(x)n_{\mathrm{II}}(x) - K_e(x - x_0), \tag{1}$$

where K_e is the force constant for the passive elastic elements (e.g., *nexin links* which may exert a restoring force proportional to their distortion), and x_0 is their location in the unstretched state.

If this functional unit is subject to internal viscous shear force, $\gamma\, \mathrm{d}x/\mathrm{d}t$ (γ is the internal viscous shear resistance*), the system obeys the force-balance equation

$$\gamma \frac{\mathrm{d}x}{\mathrm{d}t} = F. \tag{2}$$

When K_e is small enough (say 0), this system exhibits *bi-stability*. Either a stable state at $x = x_1$ or x_2 can be present, depending on the initial sliding. When x_0 is located in the unstable region and K_e is large enough, this system shows oscillations. Therefore, the functional unit has potentially excitability and oscillations.

* The internal viscous shear resistance is tentatively considered to allow force balance at a finite sliding velocity. In the flagellar and ciliary simulations, however, the internal viscosity is replaced by the external viscosity (see Eq. (3)).

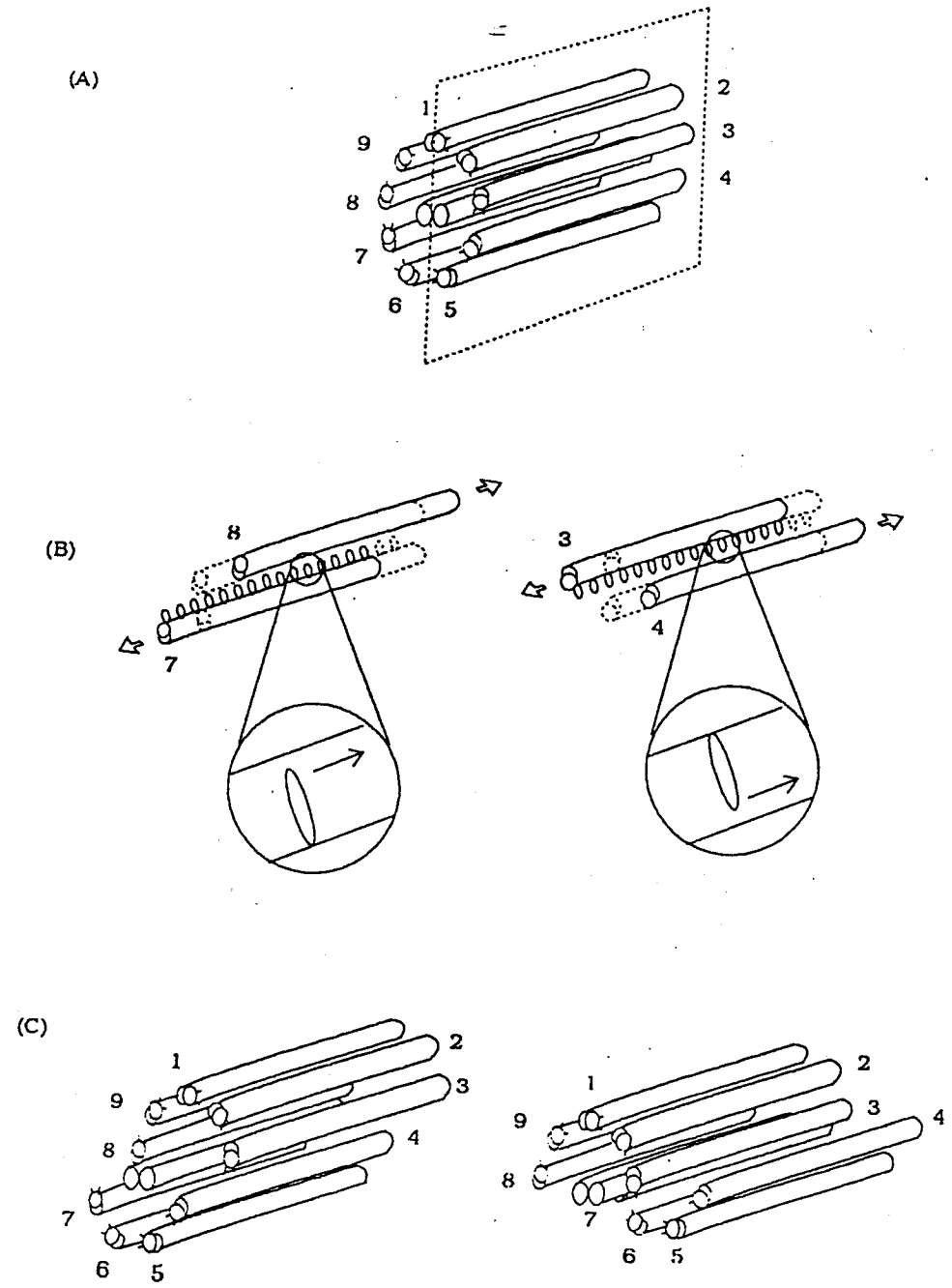

Figure 2. Structure and function of an axoneme. (A): Nine outer doublets are arranged around a central pair of singlets. This arrangement is known as the "9+2" structure. Two rows of dyneins extend from each outer doublet in a clockwise direction, when the axoneme is viewed in transverse section from the base of the organelle to its tip. If bending occurs in a single plane as indicated by dotted lines, dyneins on the left half of the axoneme are opposed to those on the right half. The two opposing halves of the axoneme refer to subsystems I and II. (B): A dynein on each doublet undergoes a undirectional power stroke as shown in the enlarged "dyneins". While active sliding caused by the dynein power stroke between doublets Nos 7 and 8 occurs in one direction (left), active sliding between doublets Nos 3 and 4 occurs in the opposite direction (right). This occurs because dyneins on the left and right halves of the axoneme have different orientations. (C): When the sliding between doublets Nos 7 and 8 in subsystem I is "active", the sliding between doublets Nos 3 and 4 in subsystem II is "passive" (left), and vice versa (right). This occurs because the axoneme has a closed ring structure.

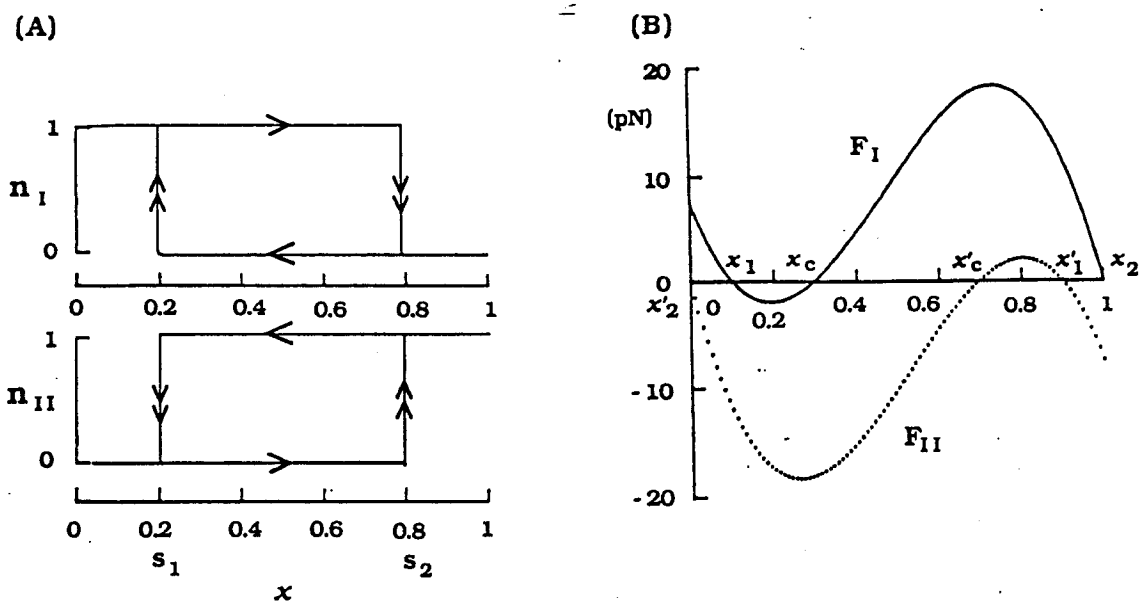

Figure 3. The hysteresis switching and cubic force-distance functions. (A): The hysteresis "on-off" switches, n_I (for subsystem I) and n_{II} (for subsystem II), are defined as a binary function of the sliding, x. (The "on" and "off" states are represented by 1 and 0 discrete values.) A dynein switches between these two states when the sliding passes critical values (called *switching points*). When the shear falls below S_1 (= 0.2) the dynein is turned "on" and maintains its state until the sliding rises above S_2 (= 0.8), and turns the dynein "off". By setting $S_1 \neq S_2$, either "on" or "off" can occur depending on the "history" of the dynein behavior. Note that $n_I + n_{II} = 1$ for each direction of movement. (B): The force generated by a dynein in the "on" state is shown as a function of the sliding, x. The solid line shows the force, F_I, for sliding in the forward direction (increasing x), and the dotted line the force, F_{II}, for sliding in the backward direction (decreasing x), which is controlled by the hysteresis switches shown in panel (A). The analytic form of F_I is:

$$F_I(x) = Q_I(x - x_1)(x - x_2)(x_c - x),$$

where Q_I (= 250 pN) is the scaling factor corresponding to the number of dyneins, x_1 (= 0.1) and x_2 (= 1) are the two stable positions and x_c (= 0.3) is a threshold position. After Murase *et al.* [32].

3. Flagellar Dynamics

A flagellum (and a cilium) can be viewed as an ensemble of a large number of functional units which are coupled through viscoelastic interactions. The motility of a flagellum in a viscous fluid is, thus, described by the fourth-order partial differential equation [32]

$$C_N \frac{\partial x}{\partial t} + \frac{\partial^2 F}{\partial s^2} + E_B \frac{\partial^4 x}{\partial s^4} = 0, \tag{3}$$

where C_N is the external viscous drag coefficient, x is the sliding (= the angle θ that the flagellum makes to a fixed external coordinate system) as a function of arc length s and time t, F is the total shear force given by Eq. (1), and E_B is the bending resistance.

In solving Eq. (3), free end boundary conditions were used at both ends, in which the external viscous forces and moments vanish:

$$\left.\frac{\partial^2 x}{\partial s^2}\right|_{s=0,L} = 0, \quad \left.\frac{\partial x}{\partial s}\right|_{s=0,L} = 0, \tag{4}$$

where L is the length of the flagellum.

Suppose we have a "homogeneous" flagellum with a length of 50 μm, in which bi-stable units are arranged along the length of the axoneme. Of course this "homogeneous" axoneme cannot develop bending waves without superthreshold perturbations if the axoneme is initially straight. However, a slightly deformed axoneme can develop bending waves. Bend propagation occurred first from base to tip (Fig. 4) and then the direction was reversed at about $t = 1120$ ms (Fig. 5). These tip-to-base propagating waves were further replaced by the base-to-tip propagating waves at about $t = 2340$. This kind of reversal of bend propagation occurred at about 1200 ms intervals as long as the computer simulation persisted (Fig. 6).

Although the "homogeneous" flagellum displayed reversal of bend propagation as observed in some species [10], [11], the problem still remaining is to clarify how

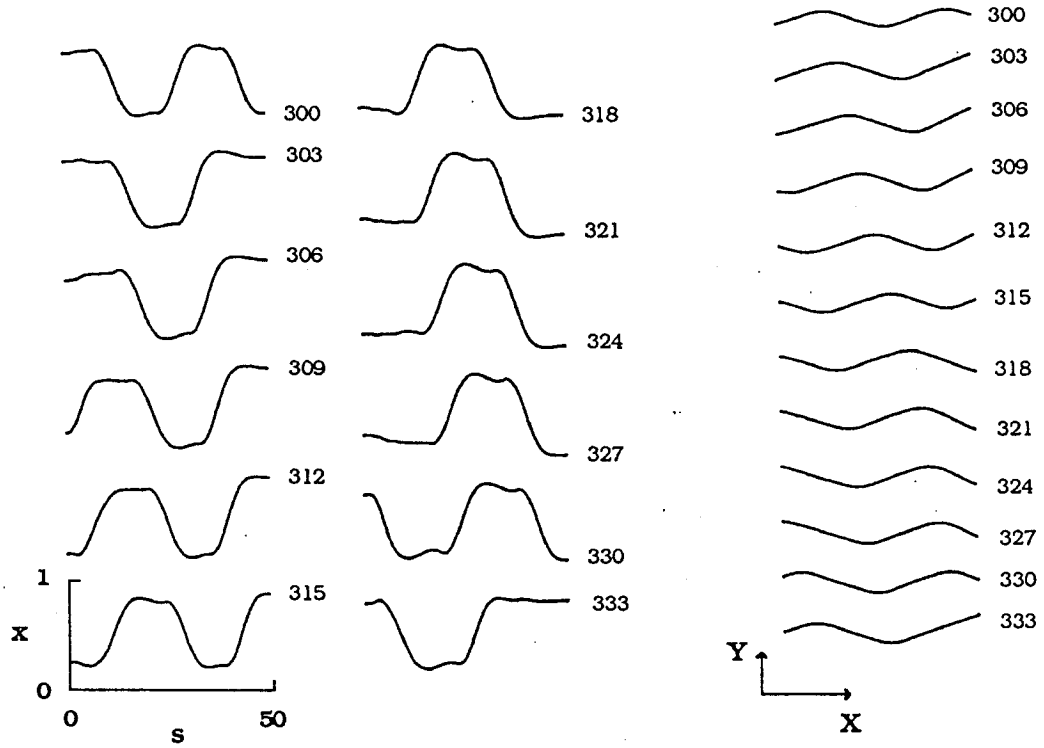

Figure 4. Symmetric base-to-tip bend propagation along a "homogeneous" axoneme under free end boundary conditions. The initially deformed axoneme was allowed to develop its bending waves. The sliding, x, is shown in ms at the indicated times on the left side of the figure, while the corresponding axonemal shapes are presented on the right side. The flagellar shapes in the (X, Y) coordinates are obtained by

$$X(s) = \int_0^s \cos(x - 0.5)\,ds, \qquad Y(s) = \int_0^s \sin(x - 0.5)\,ds.$$

For all simulations, a 50 μm long flagellum was divided into 50 segments of length 1 μm. For each segment, a functional unit modelled previously was assumed.

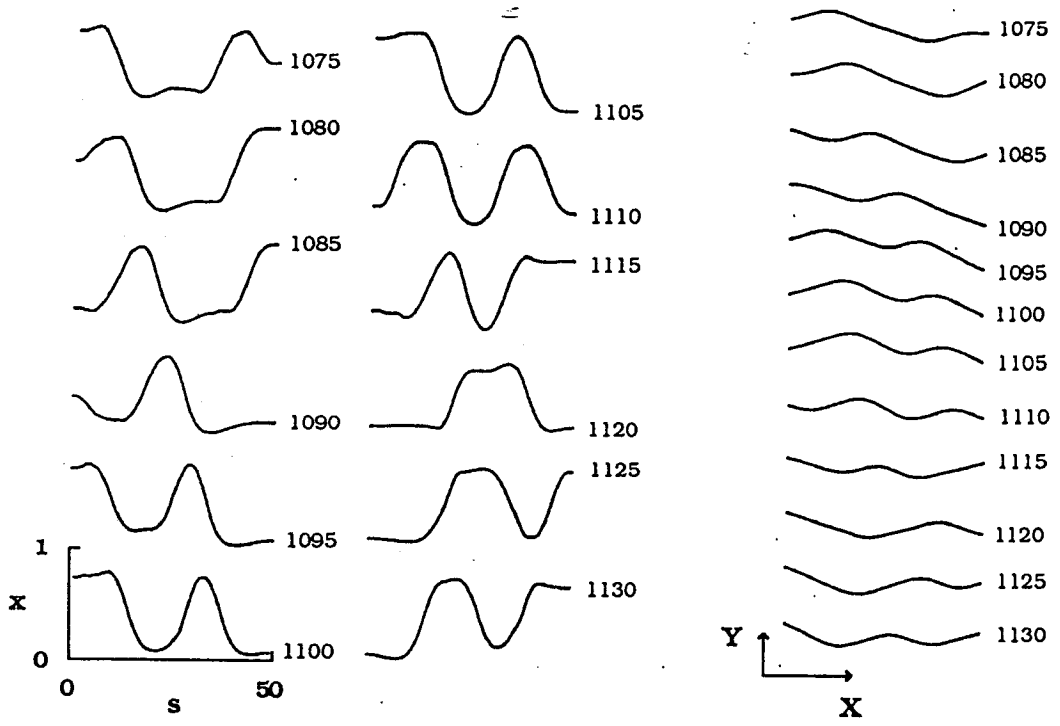

Figure 5. The reversal of the direction of propagating waves. Under the free end boundary conditions at the distal end, both the external viscous force and moment are zero, thereby the tip can move and rotate freely relative to the other regions. Once the tip happened to swing due to active sliding in the direction of increasing x ($t = 1115$ ms), it affected more proximal regions and triggered successive active sliding in the same direction via viscoelastic interactions leading to the tip-to-base propagating wave. There were two waves propagating in the opposite directions and they were slightly different with each other. When they collided ($t = 1120$ ms), only a tip-to-base propagating wave emerged from the collision.

this model displays "normal" base-to-tip bend propagation. To solve this problem, two major modifications were needed. First, a *self-oscillatory* unit was placed at the basal end. This can be achieved by increasing K_e at $s = 1\,\mu$m.* This self-oscillatory unit acts as a *pacemaker* for the flagellum. Second, a 10 μm passive terminal region was included at the tip without any dyneins. This passive region sufficiently prevents from initiating bends at the tip. After these modifications the "inhomogeneous" model displayed stable base-to-tip bend propagation (simulation not shown).

It was discovered that the frequency of the reversal of bend propagation depends on two factors: the stiffness of the basal elasticity (K_e at $s = 1\,\mu$m) and the length of the passive terminal region. Intermittent swimming patterns [12] are probably demonstrated by this class of model if we specify the two factors precisely.

It is known that real flagella of approximately 42 μm long have terminal regions of 5–8 μm [29], and that removal of the normal distal end of the flagellum interfered with its ability to generate base-to-tip propagating waves [37]. The simulation

* Real flagella and cilia have strong elastic components at the base, which may be approximated by the large K_e values at $s = 1\,\mu$m.

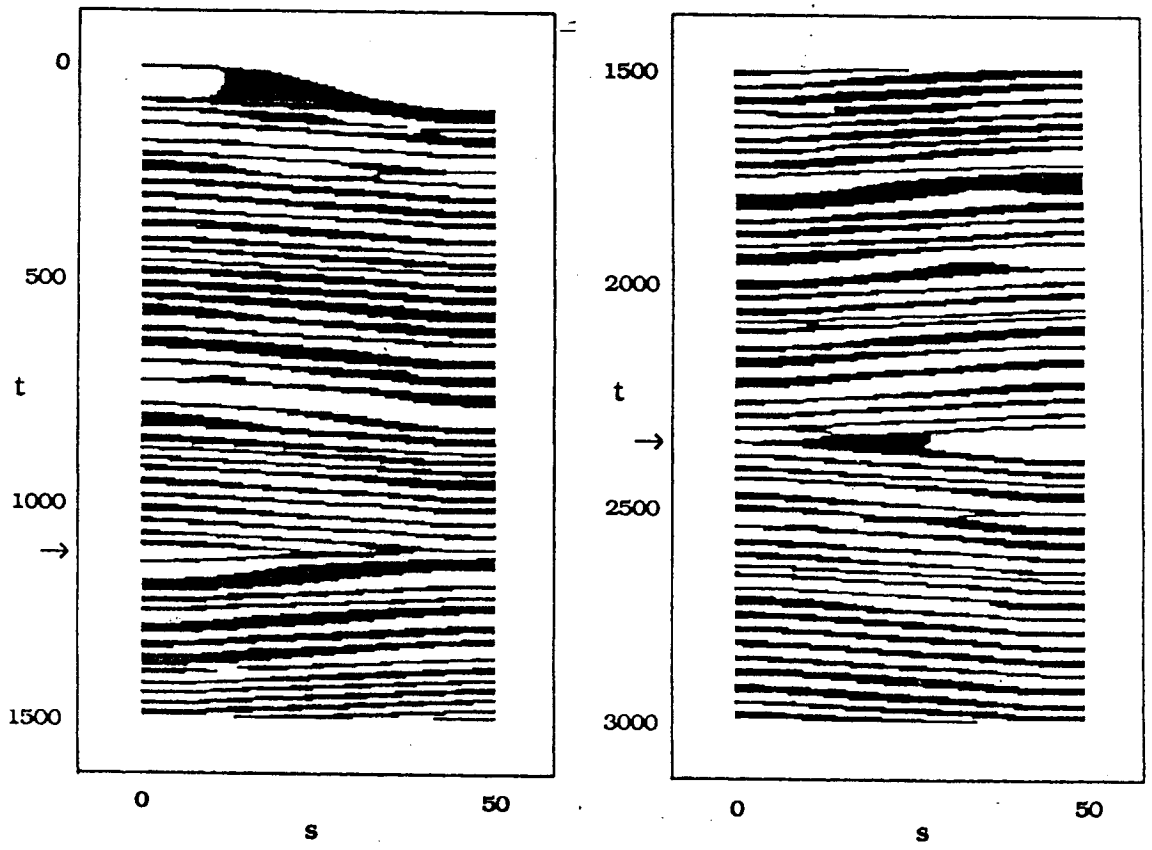

Figure 6. Positions of waves as a function of time, t (in ms), and space, s (in μm). The regions $x > 0.5$ are plotted by bars. For $0 < t < 1115$ ms, the groups of bars moved toward the right reflecting that bending waves initiated at the base (at the left end) propagated towards the tip (the right end). At $t = 1120$ ms (indicated by the first arrow), two waves propagating in the opposite directions collided. For $1120 < t < 2335$ ms, the tip-to-base bend propagation occurred. At $t = 2340$ ms (indicated by the second arrow), the direction of bend propagation was reversed again.

results presented here, as well as these experimental observation suggest that the axonemal structure is highly responsible for the dynamical behaviors.

4. Ciliary Dynamics

The ciliary model assumes the same hysteresis switching function (Fig. 7, A). For a ciliary cycle to have an alternate effective and recovery stroke, however, there must be some asymmetry between the two opposing dynein subsystems [28], [30] (Fig. 7, B). Let us define potential energy function U_{I} (or U_{II}) for subsystems I (or II). It is obtained by integrating F_{I} (or F_{II}) with respect to x (see Eq. (1)). The total potential energy function U'_{I} (or U'_{II}) is also defined as a sum of U_{I} and the potential function obtained by the integration of the elastic shear force with respect to x.* For the same reason discussed above, a cilium with a length of 10 μm is assumed to be "inhomogeneous" (Fig. 7, C).

* When K_e is small enough, there is little different between U_{I} (or U_{II}) and U'_{I} (or U'_{II}).

Boundary conditions at the distal (free) end of a cilium require Eq. (4). At the proximal end, however, the cilium is attached to the cell surface. "Pinned" boundary conditions were used, in which the velocity and moment vanish:

$$\left.\frac{\partial^3 x}{\partial s^3}\right|_{s=0} = 0, \quad \left.\frac{\partial x}{\partial s}\right|_{s=0} = 0. \tag{5}$$

Initially the cilium was straight ($\partial x/\partial s = 0$ for $0 < s < 10\,\mu$m), dyneins in subsystem I were in the "on" state for all the active region of the axoneme ($n_{\mathrm{I}} = 1$ for $0 < s < 8\,\mu$m), and all the units were in the same sliding ($x = 0.1$ for $0 < s < 10\,\mu$m).

Figure 8 shows a full cycle of the model behavior when the potential energy curve labelled 2 in Figure 7, B, was used. Panels (A) and (B) shows a recovery and an effective stroke (right) and corresponding sliding patterns plotted against space, s, and time, t, (left). In panel (C), x at $s = 5\,\mu$m is plotted as a function of time.

These simulation results are interpreted in terms of "on-off" switches and triggered events in the following way. Since initially all the dyneins in subsystems I were in the "on" state ($n_{\mathrm{I}} = 1$), the dynein in the basal region would prefer to stay at about $x = 0.75$, whereas the dynein in the rest of the active region would prefer to stay at about $x = 0.1$ (see Figure 7, B). Thus there seemed to be "mutual instability" between the basal region and the rest of the cilium with respect to the stable position of these dyneins. As a result of a strong inclination toward the stable position at about $x = 0.75$, sliding in the forward direction (increasing x) was initiated. Since there was a relatively high potential barrier (indicated by the arrow in Figure 7, B) in each dynein, active sliding was triggered successively along the axoneme. This accounts for a recovery stroke.

After the recovery stroke, dyneins in subsystem I were turned "off" and dyneins in subsystem II were turned "on". As shown in Figure 7, B, most of the active region was in a stable position (turned) at about $x = 0.9$, whereas the basal region was in a stable position at about $x = 0.3$. There appeared to be "mutual instability" again between the basal region and the rest of this system. As a result, active sliding in the backward direction (decreasing x) was initiated. Since the potential barrier in subsystem II was relatively smaller than that in subsystem I, active sliding was rapidly triggered along the axoneme. This accounts for an effective stroke. Since the system was completely reset after a full cycle, it could exhibit repetitive beat cycles as indicated by Figure 8, C.

Now consider what happens when the slope of potential energy curve is set to be high enough to prevent dyneins in subsystem I from switching "on". (Curve 1 in Figure 7, B was adopted.) The ciliary model exhibited almost the same beat cycle with a recovery and an effective stroke. After the effective stroke, however, the model stopped beating due to the failure of the switch at the basal region (cf. Fig. 9). This accounts for a quiescence of ciliary beat in a specific stroke position.

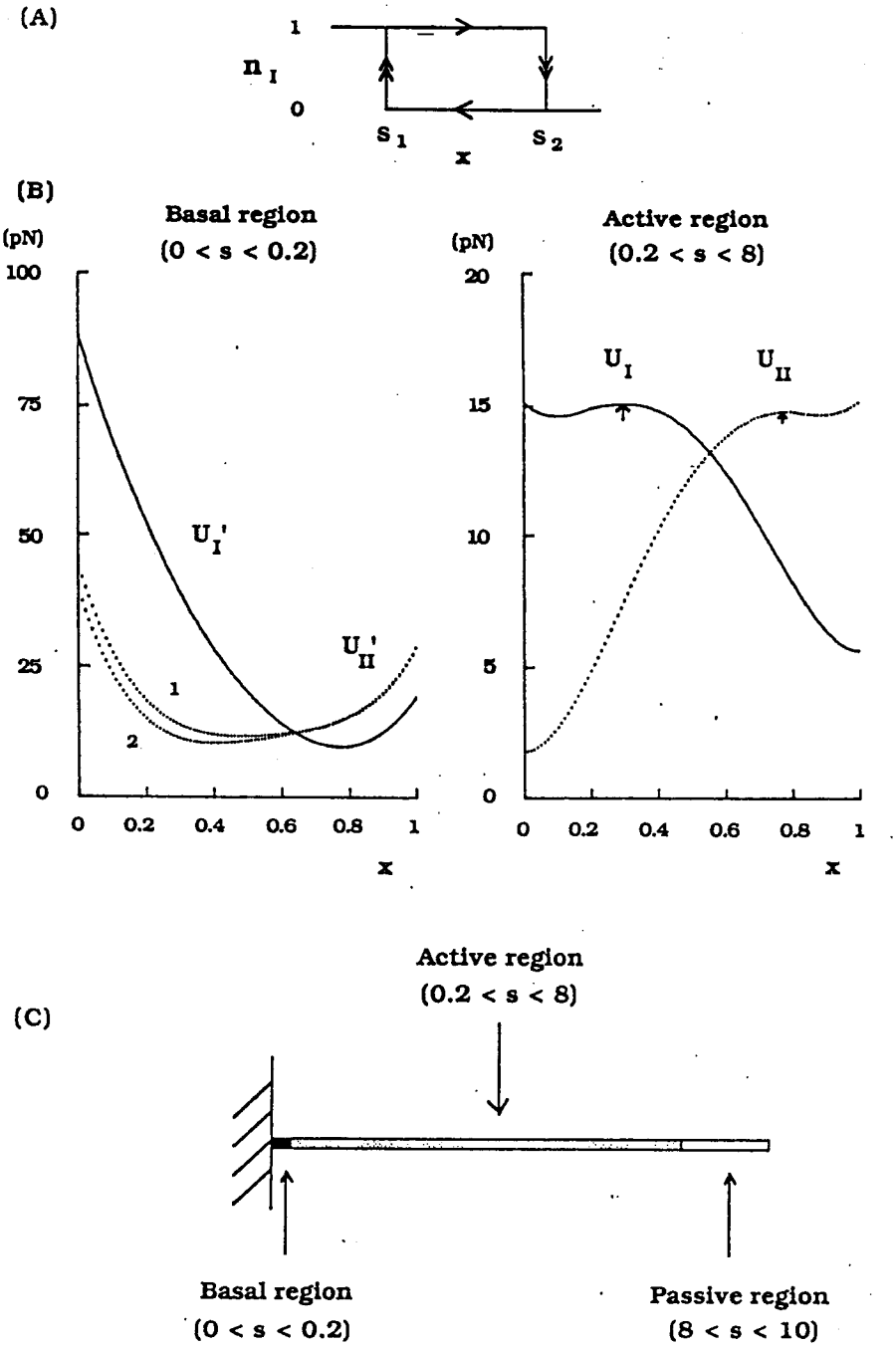

Figure 7. "Inhomogeneous" axonemal model for a cilium. (A): A hysteresis switching function for subsystem I. (B): The left panel shows the total potential energy functions U_I' and U_{II}'. The right panel shows the potential energy functions U_I and U_{II}. They are defined as follows:

$$U_i(x) = -\int_0^s F_i(x)\,ds, \qquad U_i'(x) = -\int_0^s [F_i(x) - K_e(x - x_0)]\,ds, \qquad i = \text{I, II.}$$

Since the potential energy function for a passive elastic component in the rest of the active basal region is small, U_I' and U_{II}' are almost equivalent to U_I and U_{II}. (C): A schematic representation of an "inhomogeneous" cilium. For all simulations, a 10 μm long cilium was divided into 50 segments of length 0.2 μm. There were the basal region ($0 < s < 0.2\,\mu$m), the active region ($0.2 < s < 8\,\mu$m) and passive region without dyneins ($8 < s < 10\,\mu$m). After Murase [33].

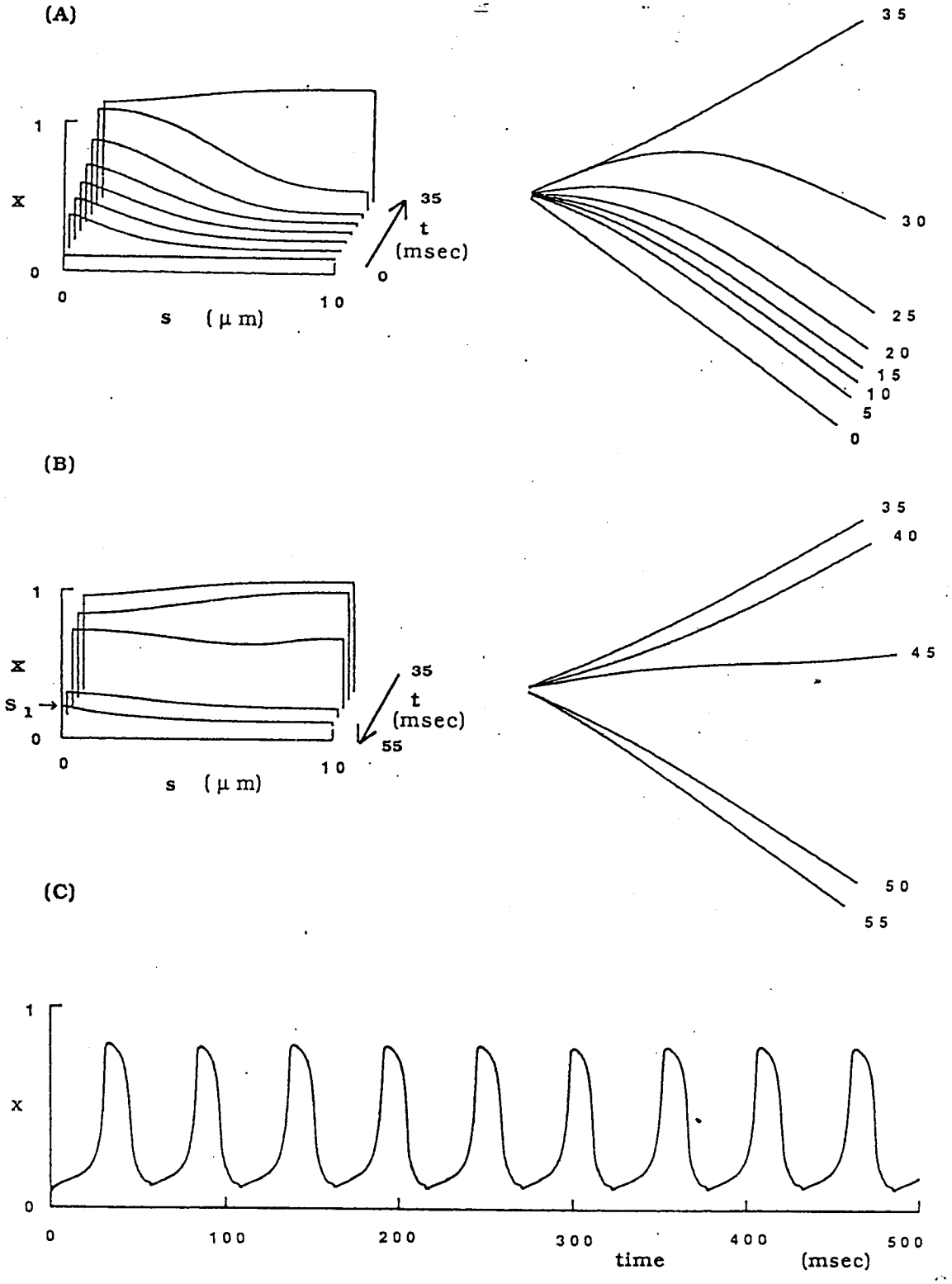

Figure 8. Repetitive beating solution of a ciliary model. Panel (A) shows a recovery stroke (right) and sliding patterns plotted as a function of space, s, and time, t (left). Panel (B) shows an effective stroke (right) and sliding patterns (left). S_1 denotes one of the switching points. After the effective stroke ($t = 55$ ms), all the units have $x < S_1$ and hence the system is completely reset. Panel (C) shows the time course of x at $s = 5\,\mu$m. The frequency of the repetitive beat cycles is 18 Hz. Curve 2 in Figure 7, B, was adopted. After Murase [33].

The question naturally arises as to whether fluid flow past a quiescent cilium might act to trigger repetitive beating. To answer this question we must modify Eq. (3) as follows:

$$C_N\left(\frac{\partial x}{\partial t} - \frac{\partial V_f}{\partial s}\right) + \frac{\partial^2 F}{\partial s^2} + E_B \frac{\partial^4 x}{\partial s^4} = 0, \tag{6}$$

where V_f is the normal component of the velocity, V, of the fluid (i.e., $V_f = V \cos\theta$, where θ is the angle between the cilium and the fixed external coordinate system).

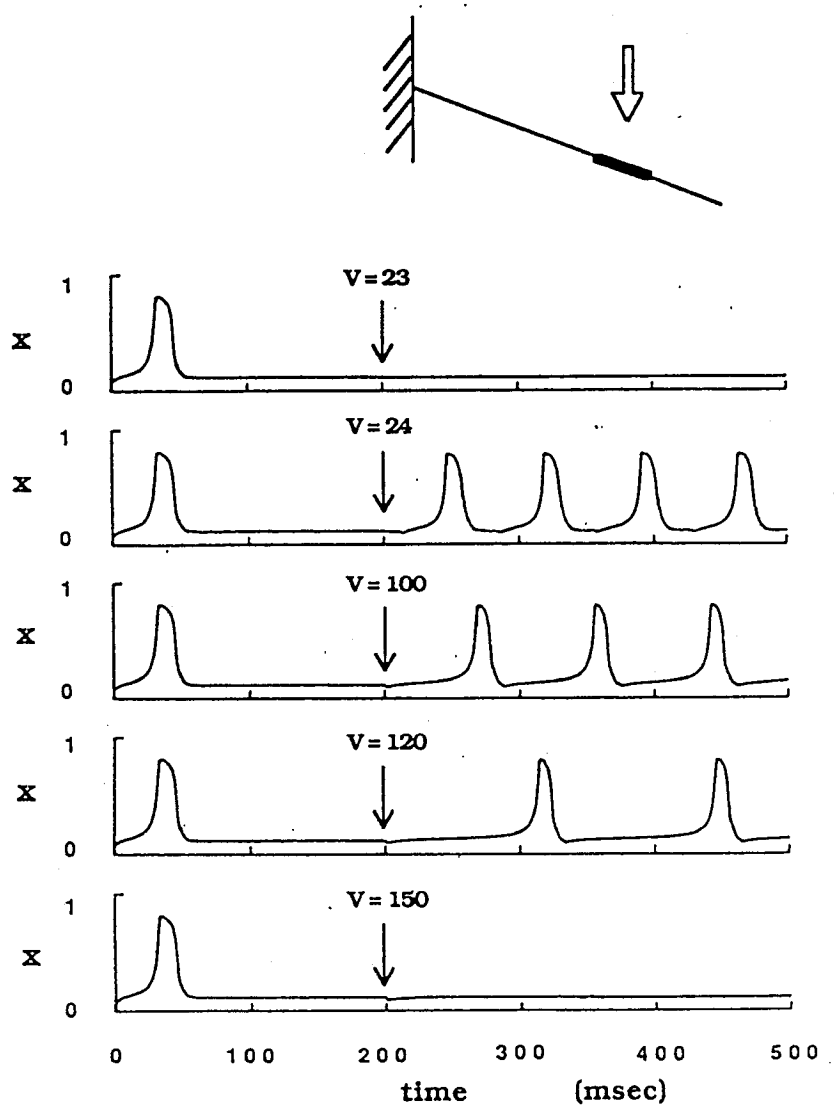

Figure 9. Effect of fluid flow on a quiescent cilium. x (at $s = 5\,\mu$m) is plotted as a function of time in order to illustrate ciliary activity. The cilium showed only a single beat and stopped at the end of the effective stroke when curve 1 in Figure 7, B, was adopted. The inset shows the position of this resting cilium, the direction of flow of a fluid with the viscosity of water and its location ($6 < s < 8\,\mu$m). Fluid flow with proper magnitude and direction can accommodate the "on-off" switches at the basal region and thus facilitate repetitive beat cycles. After Murase [33].

In the simulations shown in Figure 9, the cilium executed only a single beat, and stopped at the end of its effective stroke. The position of this resting cilium is shown in the top panel. A constant flow of water in the direction of the effective

stroke and over a particular location ($6 < s < 8$ μm) shown was then assumed to begin at $t = 200$ ms. When the fluid velocity was 23 μm/s, the cilium remained stationary. When V was increased to 24 μm/s, repetitive beating was initiated. Beat frequency was decreased with an increase in V to 100 μm/s. Thus, fluid flow above a certain threshold value can initiate a repetitive beating pattern in a cilium which would otherwise be quiescent. If fluid flow increased further, the frequency was decreased ($V = 120\,\mu$m/s) and finally the cilium cannot overcome the fluid force and hence beating creased ($V = 150\mu$m/s).

If the direction of flow of fluid was opposite to that shown, the cilium remained quiescent. Thus initiation of repetitive beating by fluid flow requires both that the speed of flow be above some threshold value and in the appropriate direction. In this sense the model cilium being quiescent at the end of the effective stroke is characterized by excitability with directional sensitivity.

5. Discussion

Spatio-temporal patterns in Figure 6 give us important insights into the complexity of the model behavior. First, the velocity of bend propagation would fluctuate as the slope of successive bars is not constant. This refers to nonuniform bend propagation in real flagella [38]. Second, the wavelength would fluctuate as the width of the bars along the s-axis is not constant. Third, the beat frequency would fluctuate as the "black-white" interval along the t-axis is not constant.

These three characteristics are not obvious as long as we take only a small number of snapshots of flagellar shape at different instants (see, e.g., the left panel of Fig. 4). Furthermore, the flagellar shapes are obtained by an integral form (see legend to Fig. 4), so that if there are spatial fluctuations on the sliding patterns they smooth away when they are transformed into shapes. For these reasons, the above characteristics have not been discussed throughly. Although experimental data showed irregularity, it was often ascribed to the nature of *random noise* [38]. However the present study suggests that these fluctuations arise in a *deterministic* mathematical model. It seems that they are not caused by random noise nor numerical errors, but are inherent in the system under the influence of external viscosity.

Now consider the origin of these "intrinsic" fluctuations based on the following fourth-order partial differential equation

$$\frac{\partial x}{\partial t} = A\frac{\partial^2 x}{\partial s^2} - B\frac{\partial^4 x}{\partial s^4} + G(x), \tag{7}$$

where x is a state variable defined at space s and time t A and B are constants, and $G(x)$ is some nonlinear function. This type of equation has been considered elsewhere [39]–[46]. The second order term in Eq. (7) corresponds to the diffusion process. When $A > 0$ spatial perturbations are stabilized (*normal diffusion*), while when $A < 0$ they are destabilized (*negative diffusion*). Suppose that the total shear force F in Eq. (3) is proportional to the sliding x. Then, Eq. (3) is analogous to Eq. (7). This situation corresponds to the case $A < 0$ and $B > 0$. The fourth order term insures the stabilization of spatial modes, while the second order term leads to destabilization. The system is characterized by *local instability* and *global stability*

leading to fluctuations. It is not surprising that the model described by Eq. (3) with nonlinear force-distance function F is subject to "intrinsic" fluctuations.

As a result of these "intrinsic" fluctuations, the "homogeneous" axoneme happened to initiate the tip-to-base propagating wave as shown in Figure 5. There were two waves with slightly different shapes propagating in the opposite directions. When they collided, one wave destroyed the other and continued to propagate after collision. If this system has two identical waves, they pass though each other on collision [32]. The nonannihilating wave phenomena of this kind are known as *soliton-like* behaviors [47].

There are only even powers of the space derivatives, so that symmetry holds with respect to space s.* It is possible that two waves propagating in the opposite directions coexist as discussed above. One way by which undirectional propagated waves are obtained is to introduce the curvature feedback control [19], [20], [22]–[27]. The curvature of the axoneme can only be defined when two separate positions are specified.** This automatically induces the spatial coordination in violation of the $s \rightarrow -s$ symmetry. Unfortunately, there is no direct experimental evidence for the curvature feedback control.

An alternative way in demonstrating undirectional bend propagation is to take into account the structural asymmetry such as the basal elastic component and the passive terminal piece. The passive region acts as a "buffer" which absorbs "intrinsic" fluctuations and also induces "polarity" of the axoneme. The present model, thus, provides a good example for studying the relationship between structure and function in cilia and flagella.

It is also interesting to note that a model cilium consisting of a series of "excitable" dyneins displays "excitability" again with directional sensitivity at the system level. If many such "excitable" celia were closely packed, the activity of adjacent cilia would be coordinated via hydrodynamic interactions to produce metachronal waves. Thus there seems to be a "functional hierarchy" in ciliated systems with respect to an "excitable" nature.

6. Conclusion

Like other nonlinear distributed systems, cilia and flagella show a large repertory of self-organizational phenomena such as regular and irregular dynamical behaviors. Previously, irregular behaviors have been studied less intensively than regular behaviors. The present theoretical studies, however, strongly suggest that rather than considering them separately, we should consider both regular and irregular behaviors as general phenomena characterized by their degree of order.

Acknowledgements

I am particularly grateful to Professor H. Shimizu who suggested to write this section. I wish to thank Professor J. J. Blum for his valuable comments.

* Both the equation and boundary conditions are invariant under the spatial inversion $s \rightarrow -s$.

** Mathematically, the curvature, $\varkappa$, is defined as a space derivative of the sliding: $\varkappa = \partial x / \partial s$.

References

[1] F. D. Warner,, in *Cilia and Flagella*, pp. 11, (Ed. M. A. Sleigh) Academic Press, London, 1974.

[2] J. Gray, *Ciliary Movement*, Cambridge Univ. Press, Cambridge, 1928.

[3] M. A. Sleigh, *The Biology of Cilia and Flagella*, Pergamon Press, exford, 1962.

[4] K. Summers and I. R. Gibbons, *Proc. Nat. Acad. Sci. USA* **68**, 3092 (1971).

[5] W. S. Sale and P. Satir, *Proc. Nat. Acad. Sci. USA* **74**, 2045 (1977).

[6] P. Satir, J. W-Steider, S. Lebduska, A. Nasr and J. Avolio, *Cell Motility* **1**, 303 (1981).

[7] A. F. Huxley, *Prog. Biophys. Biophys. Chem.* **7**, 255 (1957).

[8] M. Murase, H. Tanaka, K. Nishiyama and H. Shimizu, *J. Musc. Res. Cell Motility* **7**, 2 (1986).

[9] C. J. Brokaw, *J. Exp. Biol.* **43**, 155 (1965).

[10] M. E. J. Holwill and J. L. McGregor, *Nature*, (London), 1975.

[11] J. Alexander and R. G. Burns, *Nature*, (London), 1983.

[12] I. R. Gibbons, *J. Musc. Res. Cell Motility* **7**, 245 (1986).

[13] P. Satir, *Sci. Amer.* **231**, 44 (1974).

[14] B. H. Gibbons and I. R. Gibbons, *J. Cell Biol.* **84**, 13 (1980).

[15] E. Stommel, *J. Musc. Res. Cell Motility* **7**, 237 (1986).

[16] S. L. Tamm, *Nature*, (London), 1983.

[17] K. E. Machin, *J. Exp. Biol.* **35**, 796 (1958).

[18] K. E. Machin, *Proc. Roy. Soc.* **B158**, 88 (1963).

[19] C. J. Brokaw, *J. Exp. Biol.* **55**, 289 (1971).

[20] C. J. Brokaw, *Biophys. J.* **12**, 564 (1972).

[21] C. J. Brokaw, *Proc. Nat. Acad. Sci. USA* **72**, 3102 (1975).

[22] C. J. Brokaw, *Symp. Soc. Exp. Biol.* **35**, 313 (1982).

[23] C. J. Brokaw, *Biophys. J.* **48**, 633 (1985).

[24] C. J. Brokaw,, in *Cell Movement, Vol. 1*, pp. 267, (Eds F. D. Warner, P. Satir, I. R. Gibbons and Alan R. Liss) New York, 1989.

[25] M. Hines and J. Blum, *Biophys. J.* **23**, 41 (1978).

[26] M. Hines and J. Blum, *Biophys. J.* **25**, 421 (1979).

[27] J. Blum and M. Hines, *Quart. Rev. Biophys.* **12**, 103 (1979).

[28] R. Rikmenspoel and W. G. Rudd, *Biophys. J.* **13**, 955 (1973).

[29] R. Rikmenspoel, *J. Theor. Biol.* **96**, 617 (1982).

[30] K. Sugino and Y. Naitoh, *Nature*, (London), 1982.

[31] M. Murase and H. Shimizu, *J. Theor. Biol.* **119**, 409 (1986).

[32] M. Murase, M. Hines and J. Blum, *J. Theor. Biol.* **139**, 413 (1989).

[33] M. Murase, *J. Theor. Biol.* **146**, 209 (1990).

[34] M. Murase, *J. Theor. Biol.* **149**, 181 (1991).

[35] M. Murase, *J. Theor. Biol.* **154**, 27 (1992).

[36] M. Murase, *The Dynamics of Cellular Motility*, Wiley, Chichester, 1992.

[37] C. J. Brokaw, *J. Exp. Biol.* **45**, 113 (1966).

[38] C. J. Brokaw, *J. Exp. Biol.* **53**, 445 (1970).

[39] D. S. Cohen and J. D. Murray, *J. MAth. Biol.* **12**, 237 (1981).

[40] F. Lara Ochoa, *Biosystem* **17**, 35 (1984).

[41] J. D. Murray, *Mathematical Biology*, Springer-Verlag, Berlin, 1989.

[42] G. I. Sivashinsky, *Acta Astronautica* **4**, 1177 (1977).

[43] G. I. Sivashinsky, *Acta Astronautica* **6**, 569 (1979).

[44] D. M. Michelson and G. I. Sivashinsky, *Acta Astronautica* **4**, 1207 (1977).

[45] Y. Kuramoto, *Chemical Oscillations, Waves and Turbulence*, Springer-Verlag, Berlin, 1984.

[46] J. M. T. Tompson and L. N. Virgin, *Phys. Lett.* **A 126**, 491 (1988).

[47] H. C. Tuckwell, *SIAM J. Appl. Math.* **39**, 310 (1980).